Bin Shen
Department of Mechanical Engineering,
University of Michigan,
Ann Arbor, MI 48109

Guoxian Xiao
Manufacturing Systems Research Laboratory,
General Motors R&D,
Warren, MI 48092

Changsheng Guo
United Technologies Research Center,
East Hartford, CT 06108

Stephen Malkin
Department of Mechanical and Industrial Engineering,
University of Massachusetts,
Amherst, MA 01003

Albert J. Shih
Department of Mechanical Engineering,
University of Michigan,
Ann Arbor, MI 48109

Thermocouple Fixation Method for Grinding Temperature Measurement

A new thermocouple fixation method for grinding temperature measurement is presented. Unlike the conventional method using a welded thermocouple, this new method uses epoxy for affixing the embedded thermocouple within a blind hole in the workpiece subsurface. During grinding, the thermocouple junction is exposed and bonded to provide direct contact with the ground surface by the smearing of the workpiece material. Experiments were conducted to evaluate this simplified thermocouple fixation method including the effect of thermocouple junction size. Heat transfer models were applied to calculate the energy partition for grinding under dry, wet, and minimum quantity lubrication (MQL) conditions. For shallow-cut grinding of cast iron using a vitreous bond aluminum oxide wheel, the energy partition using a small wheel depth of cut of 10 μm was estimated as 84% for dry grinding, 84% for MQL grinding, but only 24% for wet grinding. Such a small energy partition with wet grinding can be attributed to cooling by the fluid at the grinding zone. Increasing the wheel depth of cut to 25 μm for wet grinding resulted in a much bigger energy partition of 92%, which can be attributed to fluid film boiling and loss of cooling at the grinding zone. [DOI: 10.1115/1.2976142]

1 Introduction

The grinding process generates an extremely high input of energy per unit volume of the material removed [1]. Virtually all this energy is converted to heat, which can cause high temperatures and thermal damage to the workpiece such as workpiece burn, phase transformations, undesirable residual tensile stresses, cracks, reduced fatigue strength, and thermal distortion and inaccuracies [1]. Numerous studies have reported on both the theoretical and experimental aspects of heat transfer in grinding. Early research concentrated on predicting workpiece surface temperatures in dry grinding in the absence of significant convective heat transfer [2–5]. Subsequent investigations have provided a detailed understanding of heat transfer to the workpiece, abrasive grains, grinding fluid, and the chips [6–12]. Thermal models have been developed to estimate the workpiece surface temperature, heat flux distribution in the grinding zone, fraction of energy entering the workpiece, and convective heat transfer coefficient for cooling on the workpiece surface.

Experimental investigations of heat transfer in grinding require accurate temperature measurements. Methods for temperature measurement in grinding include thermal imaging [13,14], optical fiber [15–17], foil/workpiece (single pole) thermocouple [18–22], and embedded (double pole) thermocouple [23–28]. The embedded thermocouple method is the most widely used of these techniques because of its relative simplicity, low cost, accuracy, and reliability. With this method, a double pole thermocouple is welded to the bottom of a blind hole drilled close to the ground surface from the underside of the workpiece [25,26]. Welding the small tip of a double pole thermocouple at the bottom of the small hole requires special discharge welding equipment and skills. During grinding, the thermocouple measures the temperature below the workpiece surface during successive passes until the welded junction is broken by the grinding action. Accurately determining the position of the temperature measurement below the surface being ground is complicated by its size and also the blind hole. Furthermore the embedded thermocouple and the hole can disturb the local temperature field. Therefore it is desirable to make the thermocouple and hole very small.

The present investigation was undertaken to evaluate a simpler embedded thermocouple method for grinding temperature measurement, which uses epoxy instead of welding to affix the thermocouple at the bottom of the blind hole. During grinding the thermocouple junction is exposed and bonded to the workpiece by smearing of the workpiece material, thereby providing direct contact with the workpiece surface and a direct temperature measurement at the workpiece surface. Experiments are conducted that compare the performance of epoxy fixated thermocouples with that of welded thermocouples in terms of temperature measurement and energy partition for dry grinding, wet (flood) grinding, and minimum quantity lubrication (MQL) using minuscule amounts of grinding fluid.

2 Experimental Setup

2.1 Grinding Test Setup. Straight surface plunge grinding experiments (no crossfeed) were conducted on an instrumented Chevalier Model Smart-B818 surface grinding machine using the setup shown in Fig. 1. The grinding wheel was vitreous bonded aluminum oxide (Saint-Gobain/Norton, Worcester, MA, 32A46-HVBEP) of initial diameter $d_s = 177.8$ mm and width $b_s = 12.7$ mm. The workpiece material was Dura-Bar 100-70-02 ductile iron with a carbon content of 3.5–3.9%, Rockwell hardness HRC 50, thermal conductivity of 63 W/m K, and thermal diffusivity of 1.63×10^{-7} m^2/s. The workpieces were of length 57.5 mm in the grinding direction and width $b_w = 6.5$ mm corresponding to the grinding width. Experiments were conducted without fluid (dry), under wet (flood) application conditions, and with MQL. The same fluid (5 vol % Cimtech 500 synthetic grinding fluid in water) was used both for MQL and flood application. MQL grinding utilized a special fluid application device shown in Fig. 1(*b*) provided by AMCOL (Hazel Park, MI). The flow rate was 5400 ml/min for flood (wet) grinding, but only 15 ml/min for MQL.

All experiments were conducted in the down mode with the wheel and workpiece velocities in the same direction at the grind-

Manuscript received September 22, 2007; final manuscript received June 10, 2008; published online September 11, 2008. Review conducted by Professor Shreyes N. Melkote.

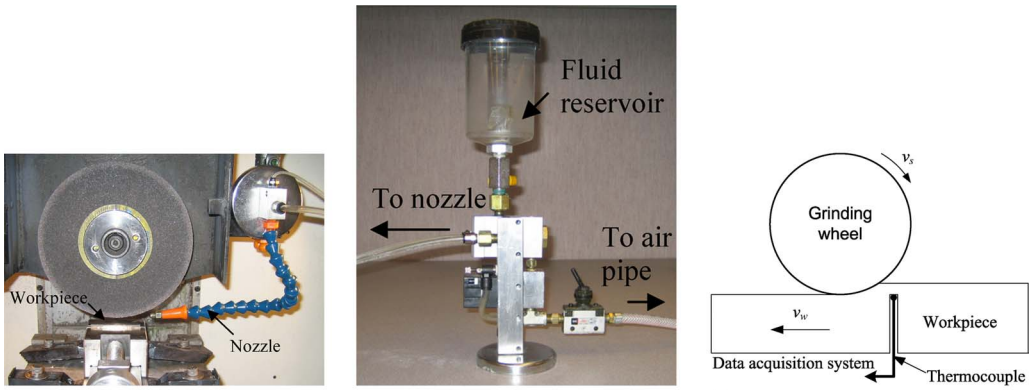

(*a*) (*b*) (*c*)

Fig. 1 Experimental setup: (*a*) overview of the setup, (*b*) MQL fluid delivery device, and (*c*) schematic drawing of grinding temperature measurement

ing zone (Fig. 1). The wheel velocity was v_s=30 m/s. Two sets of grinding parameters were used: fine grinding with a workpiece velocity of v_w=2.4 m/min and depth of cut a=10 μm and more aggressive grinding with v_w=3.0 m/min and a=25 μm. Prior to each grinding experiment, the wheel was dressed by taking a minimum of 15 passes across the rotating wheel using a rotary diamond disk dresser with a diameter of 96 mm and a width of 3.8 mm (provided by Saint-Gobain, Worcester, MA) in the up mode with a speed ratio (ratio of the peripheral dresser velocity to the wheel velocity) of −0.4, a radial depth of 10 μm, and a traverse velocity of 500 mm/min. During grinding, the normal and tangential grinding force components were measured using a Kistler Model 9257A piezoelectric dynamometer, and the temperature was measured using an epoxied or welded thermocouple (Fig. 1(*c*)). Both grinding force and temperature data were collected simultaneously at a 5 kHz sampling rate. The workpiece was allowed to cool down completely after each grinding pass.

2.2 Thermocouple Fixation. Most experiments were conducted with epoxied thermocouples, which were affixed to the bottom of a blind hole using a high temperature epoxy (Permabond 920). Both 30 and 46 gauge type K thermocouples were used to investigate the effect of junction size. The junction diameter was 0.60–0.80 mm for the 30 gauge thermocouple and 0.20–0.25 mm for the 46 gauge thermocouple. A blind hole was drilled from the underside of the workpiece to within 1–2 mm of the workpiece surface by electrical discharge machining (EDM) with a tubular electrode. The hole diameter was 0.8 mm for the 30 gauge thermocouples and 0.3 mm for the 46 gauge thermocouples. The tubular EDM electrode left a knob at the bottom of the blind hole, as shown in the cross-sectional view in Fig. 2(*a*), which made it difficult to affix the thermocouple. Therefore EDM with a solid electrode of smaller diameter was subsequently used to remove the knob and create a tapered concave pocket, as shown in Fig. 2(*b*). Figure 3(*a*) shows a cross section of the 30 gauge thermocouple junction inside a 0.8 mm diameter hole.

During grinding, the thermocouple junction is exposed (Fig. 3(*b*)), and the deformed workpiece connects the thermocouple junction to the workpiece (Fig. 4(*a*)) for temperature measurement. The sizes of the hole and thermocouple junction need to be closely matched. If the hole is too large, a good connection between the thermocouple junction and workpiece is not obtained, as seen in Fig. 4(*b*). It will be seen that this can adversely affect the temperature measurement.

The time constant of the embedded thermocouple was on the order of 1 ms [28]. Whether this response time is sufficiently fast may be ascertained by comparing it to the characteristic time it takes for a point on the workpiece surface to pass through the grinding zone, which can be calculated as the contact length l_c

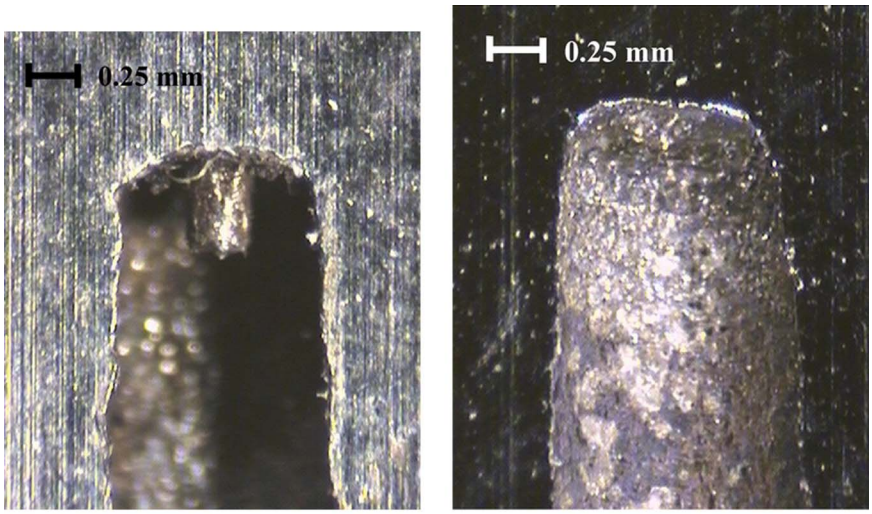

(*a*) (*b*)

Fig. 2 Cross-section view of blind hole tips: (*a*) EDM drilled using a tubular electrode and (*b*) EDM modified using a solid electrode

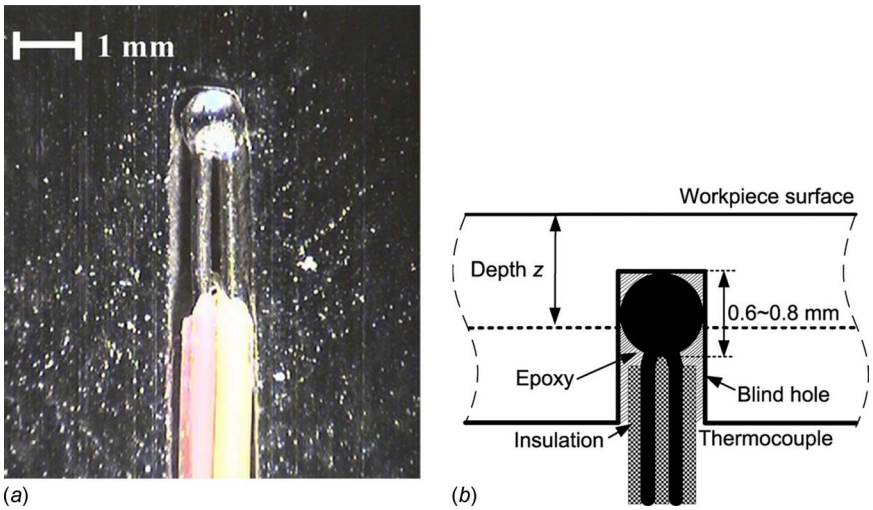

Fig. 3 Illustration of thermocouple fixation: (*a*) cross-section view and (*b*) schematic drawing

$=(\sqrt{d_s a})$ divided by the workpiece velocity v_w [28]. For the grinding conditions used in this study, the characteristic time was at least 33 ms, more than an order of magnitude longer than the time constant of the embedded thermocouple. The calibration test was conducted to verify that the epoxied thermocouple still works even after part of the junction had been ground away. For this purpose, the ground thermocouple and workpiece assembly shown in Fig. 4 was submerged in an ice-water bath (0°C) and in boiling water (100°C). Accurate temperature measurements were obtained.

For comparison, experiments were also conducted using welded thermocouples (Fig. 5). Welded thermocouples require a larger junction and a bigger hole than epoxied thermocouples, which is a definite disadvantage. Furthermore, a welded thermocouple usually breaks just as it begins to become exposed during grinding, so the maximum temperature is actually measured slightly below the ground surface. Accurately determining the temperature at the workpiece surface with a welded thermocouple is usually done by extrapolation of subsurface temperature measurements to the surface [12]. By contrast, an epoxied thermocouple maintains direct

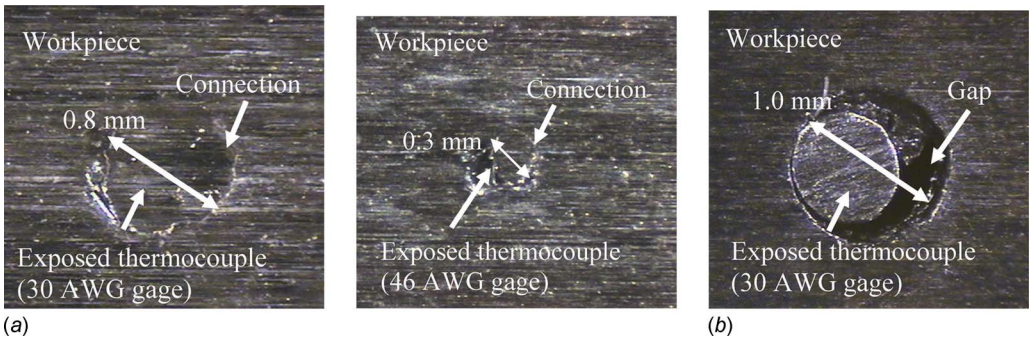

Fig. 4 Illustration of thermocouple fixation: (*a*) closely matched thermocouple tip and hole with good connection and (*b*) large hole leading to a gap surrounding the thermocouple tip

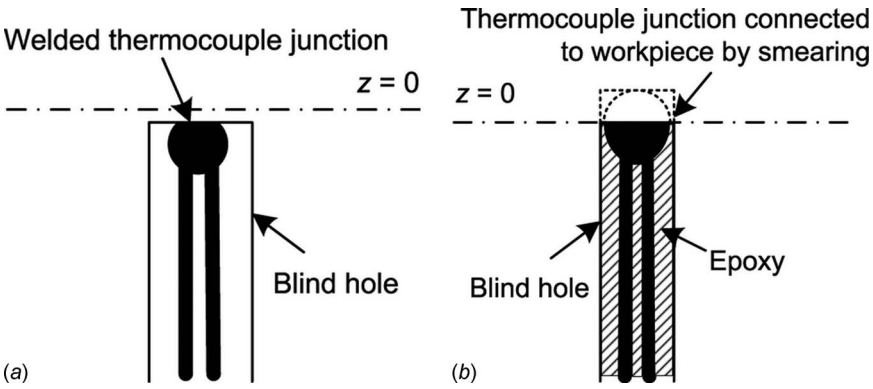

Fig. 5 Difference between (*a*) welded thermocouple and (*b*) epoxied thermocouple

Table 1 Experimental matrix design

Experiment designation	W	E1	E2	E3	ES1	ES2	EM	EW1	EW2
Fixturing method	Welded					Epoxied			
Thermocouple wire gauge	30	30	30	30	46	46	30	30	30
Depth of cut (μm)				10					25
Workpiece velocity (m/min)				2.4					3
Grinding fluid flow rate (ml/min)			N/A (dry)				15	5400	

contact with the workpiece surface as the junction is ground, thereby providing a direct measurement of the surface temperature (Fig. 4(*a*)).

2.3 Experimental Design. Grinding conditions for all experiments are listed in Table 1. Experiments with welded thermocouples are designated as Exp. W. From eight sets of experiments with epoxied thermocouples, four marked as Exps. E1, E2, ES1, and ES2 were conducted for the same grinding conditions as with the welded thermocouples. For ascertaining the effect of junction size, smaller 46 gauge thermocouples were used in Exps. ES1 and ES2. All the other experiments were conducted using 30 gauge thermocouples. One test, Exp. E3, was conducted with an epoxied thermocouple placed in an oversized hole, as seen in Fig. 4(*b*), to identify the effect of the hole diameter on the temperature measurement. Experiments EW1 and EW2 refer to wet grinding using different parameters. Experiment EM was with MQL.

3 Temperature Rise

During grinding, both the welded and epoxied thermocouples measure the temperatures at a distance z below the workpiece surface (Fig. 3(*b*)). Temperature measurements with the epoxied thermocouple in Fig. 6 show the peak temperature rise for each subsequent grinding pass progressively increasing until the thermocouple is fully exposed (Fig. 4(*a*)) and the connection between the thermocouple junction and workpiece is established. At this point the peak temperature rise is reached, and it remains nearly constant for a number of additional grinding passes. The location of the reference surface at $z=0$ can be defined by where this steady-state period begins, as illustrated in Fig. 6. The steady-state period in Fig. 6 persists for more passes with the bigger 30 gauge thermocouple than with the smaller 46 gauge thermocouple.

For a welded thermocouple, the reference of $z=0$ is usually defined at the position where the thermocouple begins to be exposed and the maximum peak temperature rise is measured [12]. However, this peak temperature probably occurs slightly below the surface since the next grinding pass usually damages the welded connection between the thermocouple and the workpiece.

Measured temperature rises for dry grinding conditions are presented in Fig. 7. For all experiments, the peak temperature is bigger closer to the surface at smaller depth z. Note that when the thermocouple is further down below the ground surface ($z \geq 0.2$ mm), the temperature measured using the welded thermocouple (Exp. W) decreases faster than the temperature measured using the epoxied thermocouple, which suggests poor thermal contact with the epoxied thermocouple. When grinding at the surface where $z=0$, good contact is obtained between the workpiece surface and epoxied thermocouple (see Fig. 4(*a*)). This can explain why the maximum temperature measured using an epoxied thermocouple is higher than for the welded thermocouple under the same grinding conditions, except for Exp. E3 (small thermocouple in a large hole) where a gap exists between the thermocouple junction and the workpiece (Fig. 4(*b*)). The lower temperature measured with the welded thermocouple is a further indication that its maximum peak temperature is measured below the surface just as the junction begins to be exposed. The data obtained with the smaller 46 gauge thermocouples in Exps. ES1 and ES2 generally show a faster response as well as a faster cooling rate than with the bigger 30 gauge thermocouples in Exps. E1, E2, and E3. This can be attributed to reduced size and lower thermal inertia.

A comparison of grinding temperatures measured at the surface ($z=0$) under dry conditions is presented in Fig. 8. The peak temperature rises for Exps. E1 and E2 are almost identical at 500°C. The peak temperature rises for Exps. ES1 and ES2 (smaller 46 gauge thermocouples) are slightly higher, 525°C and 511°C, respectively, which can again be attributed to the smaller junction size. The welded thermocouple (Exp. W) gives a lower peak tem-

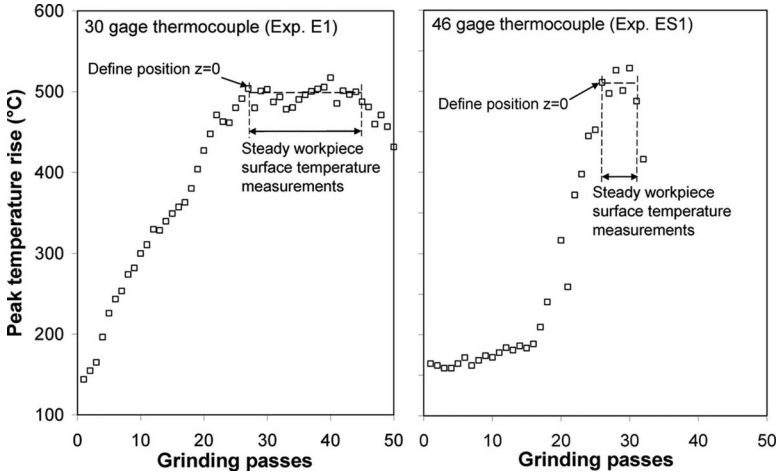

Fig. 6 Peak temperature rise versus grinding passes for epoxied thermocouple method

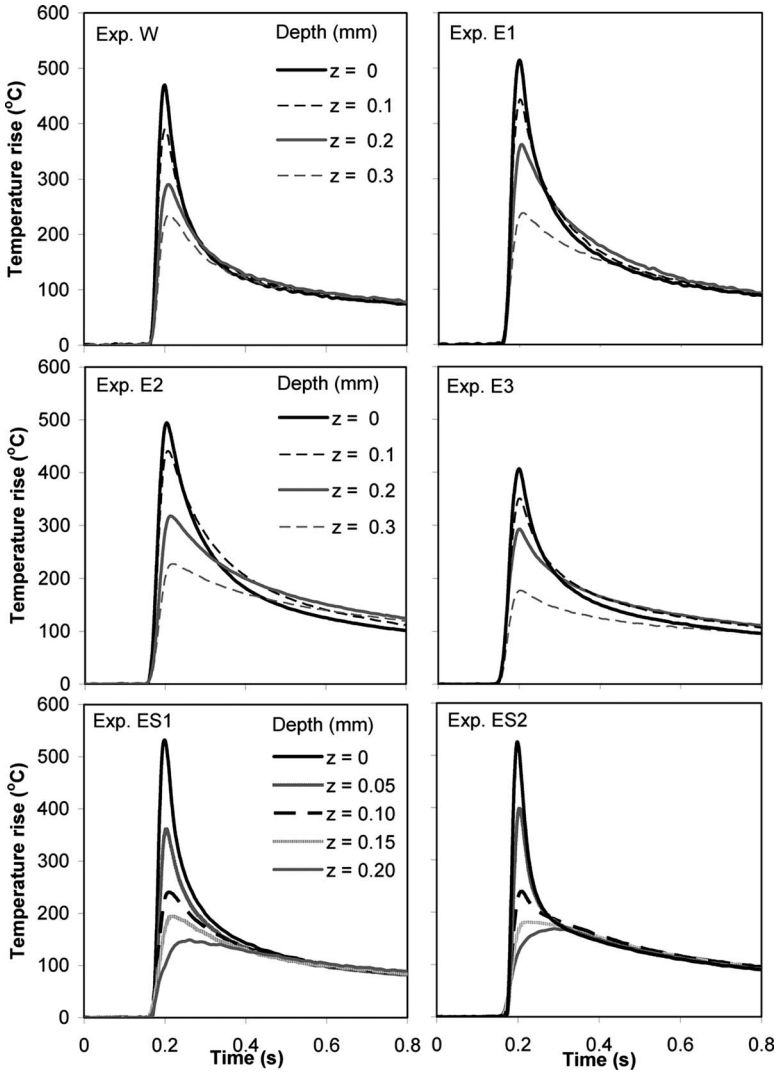

Fig. 7 Temperature rise at different depths in dry grinding: Exp. W with welded thermocouple (30 gauges), Exps. E1, E2, and E3 with epoxied thermocouple (30 gauges), and Exps. ES1 and ES2 with epoxied thermocouple (46 gauges)

perature rise (469°C), apparently because of its larger size and also damage to the weld joint, as described above. Also the welded thermocouple requires a larger hole diameter (1.5 mm) for electrical insulation, which could also lower the measured temperature. For Exp. E3 with the bigger hole, the thermal connection is not formed (Fig. 4(*b*)) and the measured peak temperature is much lower (405°C).

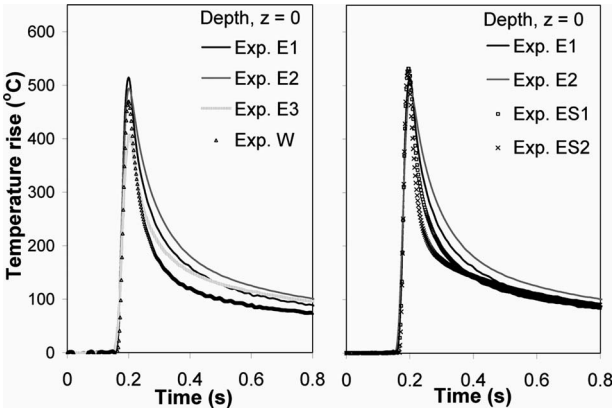

Fig. 8 Measured grinding temperature at the workpiece surface at depth $z=0$ (dry condition)

Experiment EW1 was conducted under wet conditions with the same grinding parameters as in dry grinding, but the maximum temperature rise of 106°C (Fig. 9(*a*)) was much lower. This temperature rise is comparable to or slightly less than the film boiling temperature of the water-based grinding fluid. In the absence of film boiling, the grinding fluid should provide significant cooling at the grinding zone, which is usually much more likely with creep feed grinding than with conventional shallow-cut grinding [29]. In another wet grinding test Exp. EW2 under more aggressive conditions ($v_w=3$ m/min and $a=25$ μm), the peak temperature rise (474°C) greatly exceeded the film boiling temperature of the grinding fluid.

The temperature rise for Exp. EM with MQL is shown in Fig. 10. The peak temperature rise of 444°C is about 60°C lower than for dry grinding (see Fig. 8). This lower temperature can be attributed, at least in part, to lubrication by MQL, which reduced the average tangential grinding force per unit width, F_t/b_w, from about 2.0 N/mm with dry grinding to 1.8 N/mm with MQL.

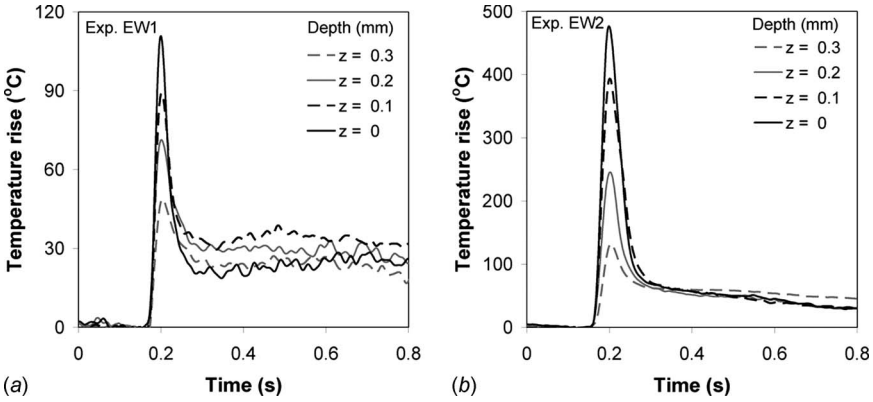

Fig. 9 Temperature rise in wet grinding at different grinding conditions: (*a*) depth of cut $a=10$ μm and workpiece velocity $v_w=2.4$ m/min and (*b*) $a=25$ μm and $v_w=3$ m/min

4 Energy Partition

4.1 Heat Transfer Models. Straight surface grinding experiments were conducted, as shown in Fig. 11, where a wheel of diameter d_s rotating with a peripheral velocity v_s removes a depth a of the material from the workpiece as it passes under the wheel at velocity v_w. Virtually all the grinding energy expended at the grinding zone is converted to heat, which is transported to the workpiece, grinding wheel, chips, and grinding fluid. The geometrical grinding zone is the region of contact length l_c where the wheel interacts with the workpiece.

The temperatures generated at the grinding zone can be calculated by considering the grinding zone as a band source of heat of length l_c, which moves along the surface of the workpiece at the workpiece velocity v_w [1]. A critical parameter for this thermal analysis is the energy partition ε, which is defined as the fraction of the grinding energy transported as heat to the workpiece at the grinding zone. Since the maximum grinding zone temperature rise $\theta_{\max}$ is measured and the total energy input can be readily calculated from the tangential force measurement, the thermal analysis can be used to evaluate the energy partition that occurred for grinding using the relationships [30]

$$q = \frac{k_w v_w^{1/2}}{\beta \alpha_w^{1/2} a^{1/4} d_s^{1/4}} \theta_{\max} \tag{1}$$

$$\varepsilon = q / \frac{F_t v_s}{b_w l_c} \tag{2}$$

where q is the heat flux into the workpiece, k_w is the workpiece thermal conductivity, α_w is the thermal diffusivity of the workpiece, F_t is the tangential grinding force, b_w is the width of the workpiece, and β is a constant that depends on the heat source shape. In this study, $\beta=1.06$ for the triangular shape heat source [30].

Guo and Malkin [11,12] developed an inverse heat transfer model based on the moving heat source theory [31]. A matrix is constructed as a function of depth z, process parameters, and workpiece thermal properties. The heat flux distribution q_i is linked to the temperature rise θ_j by the matrix c_{ji} [11,12]:

$$\sum_{i=1}^{n} c_{ji} q_i = \theta_j, \quad i,j = 1,2,\ldots,n \tag{3}$$

The grinding temperatures can be predicted by assuming the energy partition and the heat flux distribution. Alternatively the energy partition and heat flux distribution can be estimated by measuring the grinding temperature.

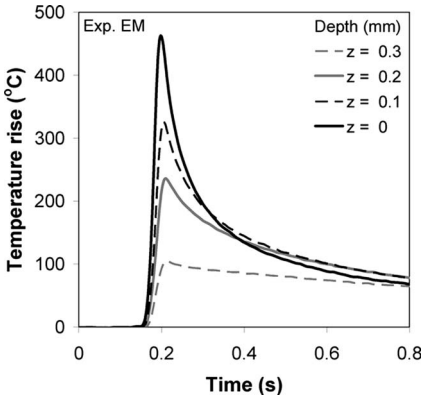

Fig. 10 Temperature rise at different depths in MQL grinding (grinding fluid flow rate=15 ml/min)

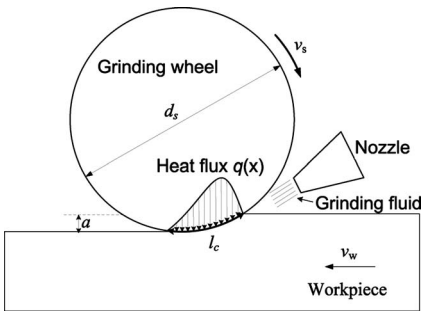

Fig. 11 Schematic drawing of heat transfer in down grinding

4.2 Energy Partition by Curve Fitting. Experimental measurements of peak temperature rise versus depth z are plotted in Fig. 12. In each case, the peak temperature rise increases closer to the surface. The inverse heat transfer model can be used to predict grinding temperature profiles at different depths. Therefore, the energy partition can be determined by matching the peak temperatures at different depths for the measured temperatures and the theoretical results. A MATLAB program was developed for obtaining a least squares fit. The energy partition calculated using this method is designated as $\varepsilon_{\text{fitting}}$.

For the welded thermocouple (Exp. W), it was found that $\varepsilon_{\text{fitting}}=72\%$ using the least squares fit over the entire range, as illustrated in Fig. 12. However, the epoxied thermocouple undermeasures the temperature when it is positioned far below the workpiece surface, due to the poor thermal contact as mentioned

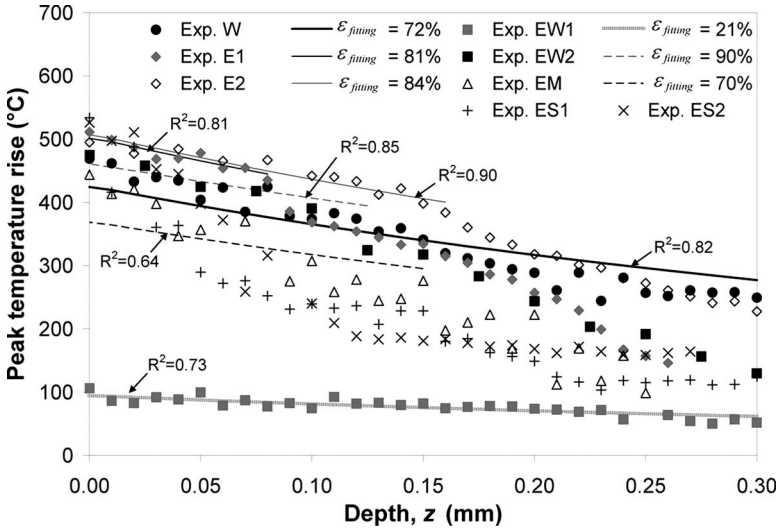

Fig. 12 Experimental and theoretical maximum temperature rise versus the depth *z*

in Sec. 3. Consequently, not all the experimental data points ranging from $z=0$ to $z=0.3$ mm are appropriate for curve fitting. Therefore, the R^2 value, which determines the goodness of fit, was used to select a cutoff depth z_0, i.e., data with depth $z<z_0$, to maximize the R^2 value. The best fit theoretical curves and their corresponding R^2 value for the epoxied thermocouple experiments are plotted in Fig. 12. The R^2 value (=0.82) for the welded thermocouple is included for comparison.

The data for the 30 gauge epoxied thermocouples, except for Exp. EW1, match well with theoretical curves only near the workpiece surface (cutoff depth $z_0 \leq 0.15$ mm). Experiments E1, E2, and EM give $\varepsilon_{\text{fitting}}=81\%$, $\varepsilon_{\text{fitting}}=84\%$, and $\varepsilon_{\text{fitting}}=70\%$, respectively. However, the R^2 value for Exp. EM (=0.64) is lower than for the other experiments. Apparently the temperature measurements in Exp. EM have a larger variation than the others due to discontinuous fluid delivery using the MQL device with 1–2 Hz pulsed fluid delivery. For Exp. EW1, the temperature rise is below the fluid burn-out limit of about 120°C. A theoretical curve with $\varepsilon_{\text{fitting}}=21\%$ matches the data fairly well over the whole range ($z_0=0.3$ mm) with $R^2=0.73$. Such a low energy partition in this case indicates effective cooling by the fluid at the grinding zone, as previously mentioned. For more aggressive wet grinding, Exp. EW2, the temperature at the grinding zone was much higher than the burn-out limit, so cooling at the grinding zone should have been ineffective. This can account for the much higher energy partition of $\varepsilon_{\text{fitting}} \approx 90\%$.

By contrast, the data obtained with the 46 gauge epoxied thermocouple (Exps. ES1 and ES2) do not match any theoretical curves ($R^2 \ll 1$). In these cases, the measured temperature is very low far below the ground surface. Apparently the small thermocouple junction fits loosely in the blind hole, leading to a much larger contact thermal resistance. Nonetheless, when the connection between the thermocouple junction and the workpiece starts to form during grinding ($z<0.04$ mm), the measured temperature increases substantially, as seen in Fig. 12.

4.3 Energy Partition Results by Surface Temperature Matching. One important advantage with epoxied thermocouples is that temperature measurements can be directly obtained at the workpiece surface, as seen in Fig. 6. Therefore it should be possible to use these peak surface temperature measurements to obtain more precise estimations of the energy partition values by matching the average of these peak temperature rises with the theoretical values according to either the simple heat transfer analysis (Eqs. (1) and (2)) or the inverse heat transfer model (Eqs. (2) and (3)). Again for this purpose, a triangular heat source was assumed. For the welded thermocouple, only the peak temperature rise at depth $z=0$ was used to calculate the energy partition since only one temperature measurement at the workpiece surface was available.

The results are summarized in Table 2, which also includes corresponding values for the specific tangential force, grinding power, and heat flux to the workpiece at the grinding zone. The energy partitions obtained with both heat transfer models ($\varepsilon_{\text{simple}}$

Table 2 Summary of heat transfer analysis in grinding experiments

Exp.	W	E1	E2	ES1	ES2	EW1	EW2	EM
Fixturing method	Welded				Epoxied			
Thermocouple wire gauge	30	30	30	46	46	30	30	30
Maximum temperature rise (°C)	469	493	503	525	511	106	474	444
Specific tangential force F_t (N/mm)	2.00	2.05	2.09	1.96	2.00	1.50	2.40	1.79
Grinding power (W)	390	400	408	382	390	293	468	349
$\varepsilon_{\text{simple}}$, simple model[a]	78%	80%	80%	89%	85%	24%	92%	83%
$\varepsilon_{\text{inverse}}$, inverse heat transfer[b]	79%	82%	82%	90%	87%	24%	93%	84%
$\varepsilon_{\text{fitting}}$, curve fitting	72%	81%	84%	--	--	21%	90%	70%
R^2 for the curve fitting	0.82	0.89	0.90	--	--	0.73	0.85	0.64
Heat flux into workpiece (W/mm^2)	36.2	38.3	39.1	40.5	39.7	8.3	51.2	34.5

[a]Reference [1].
[b]References [11,12].

and $\varepsilon_{inverse}$) are almost identical, and they are also very close to the values obtained by curve fitting ($\varepsilon_{fitting}$) with high R^2 values ($R^2 > 0.8$). When the R^2 value is lower, the estimated ε is less accurate. For Exp. EM, with $R^2 = 0.64$, $\varepsilon_{fitting}$ is about 14% lower than the values obtained with both heat transfer models. Slightly higher energy partitions were obtained with the epoxied thermocouples (Exps. E1 and E2) than with the welded thermocouple (Exp. W) because the epoxied thermocouples indicate slightly higher surface temperatures. Likewise higher energy partitions are also obtained with smaller epoxied thermocouples (Exps. ES1 and ES2) than with larger ones (Exps. E1 and E2). The very low energy partition of only 24% for the fine wet grinding test, Exp. EW1, can be attributed mainly to effective cooling at the grinding zone below the film boiling temperature, as previously indicated. With more aggressive wet grinding (Exp. EW2), the grinding zone temperature greatly exceeded the fluid film boiling temperature, cooling at the grinding zone became insignificant. The estimated energy partition of 84% for MQL grinding, Exp. EM, is almost identical to the energy partition for dry grinding, so it can be concluded that the minute amount of fluid applied by MQL provides virtually no cooling at the grinding zone.

5 Conclusions

A new thermocouple fixation method was developed for grinding temperature measurement, which uses epoxy instead of spot welding to affix the tip of the thermocouple to the bottom of a blind hole. Experiments were conducted to compare the performance of epoxied and welded thermocouples. For epoxied thermocouples, good thermal contact was obtained as the thermocouple junction became exposed by smearing of the workpiece material during grinding, thereby providing direct measurement of the surface temperature at the grinding zone. For welded thermocouples, the junctions tend to be damaged during grinding as they become exposed and the maximum temperatures are slightly smaller than the temperatures measured with epoxied thermocouples.

Grinding experiments and heat transfer analyses showed that grinding fluids provide negligible cooling within the grinding zone as evidenced by the high energy partitions, which ranged from 84% to 92% for dry grinding, wet grinding, and MQL grinding. An exception was observed for fine wet grinding, which gave a much lower energy partition of 24%, due to cooling within the grinding zone below the film boiling temperature. Although cooling by the fluid may be ineffective within the grinding zone, cooling can occur outside the grinding zone, as evidenced by the much faster drop in the measured temperature from its peak value with wet grinding (Fig. 9) than with dry grinding (Fig. 8). Bulk cooling of the workpiece in this way can be an important factor in controlling thermally induced dimensional inaccuracy and distortion. While MQL is effective in providing lubrication, it can be seen by comparing the temperature response curves for MQL (Fig. 10) with those for dry grinding (Fig. 9) that the miniscule amount of applied fluid with MQL does not provide any significant cooling outside the grinding zone. This is a major drawback that can limit the more widespread application of MQL for grinding.

Acknowledgment

This research was sponsored by National Science Foundation DMII Grant No. 0422947 and General Motors Research. Support from Saint-Gobain and AMCOL Corporation is greatly appreciated. The authors also thank Alan Rakouskas at University of Massachusetts Amherst for his assistance with thermocouple welding.

References

[1] Malkin, S., 1989, *Grinding Technology: Theory and Applications of Machining With Abrasives*, Wiley, New York, reprinted by SME, 1996.
[2] Outwater, J. O., and Shaw, M. C., 1952, "Surface Temperatures in Grinding," Trans. ASME, **74**, pp. 73–86.
[3] Hahn, R. S., 1956, "The Relation Between Grinding Conditions and Thermal Damage in the Workpiece," Trans. ASME, **78**, pp. 807–812.
[4] Takazawa, K., 1966, "Effects of Grinding Variables on the Surface of Hardened Steel," Bull. Jpn. Soc. Precis. Eng., **2**, pp. 14–21.
[5] Malkin, S., and Anderson, R. B., 1974, "Thermal Aspects of Grinding. Part I: Energy Partition," ASME J. Eng. Ind., **96**, pp. 1177–1183.
[6] DesRuisseaux, N. R., and Zerkle, R. D., 1970, "Thermal Analysis of the Grinding Process," ASME J. Eng. Ind., **92**, pp. 428–434.
[7] Lavine, A. S., 1988, "A Simple Model for Convective Cooling During the Grinding Process," ASME J. Eng. Ind., **110**, pp. 1–6.
[8] Demetriou, M. D., and Lavine, A. S., 2000, "Thermal Aspects of Grinding, the Case of Upgrinding," ASME J. Manuf. Sci. Eng., **122**, pp. 605–611.
[9] Shaw, M. C., 1990, "A Simplified Approach to Workpiece Temperature in Fine Grinding," CIRP Ann., **39**, pp. 345–347.
[10] Ju, Y., Farris, T. N., and Chandrasekar, S., 1998, "Theoretical Analysis of Heat Partition and Temperatures in Grinding," ASME J. Tribol., **120**, pp. 789–794.
[11] Guo, C., and Malkin, S., 1996, "Inverse Heat Transfer Analysis of Grinding, Part I: Methods," ASME J. Eng. Ind., **118**, pp. 137–142.
[12] Guo, C., and Malkin, S., 1996, "Inverse Heat Transfer Analysis of Grinding, Part II: Applications," ASME J. Eng. Ind., **118**, pp. 143–149.
[13] Hwang, J., Kompella, S., Chandrasekar, S., and Farris, T. N., 2003, "Measurement of Temperature Field in Surface Grinding Using Infra-Red (IR) Imaging System," ASME J. Tribol., **125**, pp. 377–383.
[14] Sakagami, T., Madhavan, V., Harish, G., Krishnamurthy, K., Ju, Y., Farris, T. N., and Chandrasekar, S., 1998, "Full-Field IR Measurement of Subsurface Grinding Temperatures," Proc. SPIE, **3361**, pp. 234–245.
[15] Ueda, T., 1986, "Measurement of Grinding Temperature Using Infrared Radiation Pyrometer With Optical Fiber," ASME J. Eng. Ind., **108**, pp. 241–247.
[16] Ueda, K. Y., and Sugita, T., 1992, "Measurement of Grinding Temperature of Ceramics Using Infrared Radiation Pyrometer With Optical Fiber," ASME J. Eng. Ind., **114**, pp. 317–321.
[17] Curry, A. C., Shih, A. J., Scattergood, R. O., Kong, J., and McSpadden, S. B., 2003, "Grinding Temperature Measurements in Mgo PSZ Using Infrared Spectrometry," J. Am. Ceram. Soc., **86**, pp. 333–341.
[18] Rowe, W. B., Black, S. C. E., and Mills, B., 1996, "Temperature Control in CBN Grinding," Int. J. Adv. Manuf. Technol., **12**, pp. 387–392.
[19] Xu, X., Yu, Y., and Huang, H., 2003, "Mechanisms of Abrasive Wear in the Grinding of Titanium (TC4) and Nickel (K417) Alloys," Wear, **255**, pp. 1421–1426.
[20] Huang, H., and Xu, X. P., 2004, "Interfacial Interactions Between Diamond Disk and Granite During Vertical Spindle Grinding," Wear, **256**, pp. 623–629.
[21] Batako, A. D., Rowe, W. B., and Morgan, M. N., 2005, "Temperature Measurement in High Efficiency Deep Grinding," Int. J. Mach. Tools Manuf., **45**, pp. 1231–1245.
[22] Lefebvre, A., Vieville, P., Lipinski, P., and Lescalier, C., 2006, "Numerical Analysis of Grinding Temperature Measurement by the Foil/Workpiece Thermocouple Method," Int. J. Mach. Tools Manuf., **46**, pp. 1716–1726.
[23] Littman, W. E., and Wulff, J., 1955, "The Influence of the Grinding Process on the Structure of Hardened Steel," Trans. Am. Soc. Met., **47**, pp. 692–714.
[24] Kohli, S. P., Guo, C., and Malkin, S., 1995, "Energy Partition for Grinding With Aluminum Oxide and CBN Abrasive Wheels," ASME J. Eng. Ind., **117**, pp. 160–168.
[25] Guo, C., Wu, Y., Varghese, V., and Malkin, S., 1999, "Temperatures and Energy Partition for Grinding With Vitrified CBN Wheels," CIRP Ann., **48**, pp. 247–250.
[26] Upadhyaya, R. P., and Malkin, S., 2004, "Thermal Aspects of Grinding With Electroplated CBN Wheels," ASME J. Manuf. Sci. Eng., **126**, pp. 107–114.
[27] Kim, H. J., Kim, N. K., and Kwak, J. S., 2006, "Heat Flux Distribution Model by Sequential Algorithm of Inverse Heat Transfer for Determining Workpiece Temperature in Creep Feed Grinding," Int. J. Mach. Tools Manuf., **46**, pp. 2086–2093.
[28] Xu, X. P., and Malkin, S., 2001, "Comparison of Methods to Measure Grinding Temperatures," ASME J. Manuf. Sci. Eng., **123**, pp. 191–195.
[29] Fuh, K. H., and Huang, J. S., 1994, "Thermal Analysis of Creep-Feed Grinding," J. Mater. Process. Technol., **43**, pp. 109–124.
[30] Guo, C., and Malkin, S., 1992, "Heat Transfer in Grinding," J. Mater. Process. Manuf. Sci., **1** pp. 16–27.
[31] Jaeger, J. C., 1942, "Moving Sources of Heat and the Temperature at Sliding Contacts," J. Proc. R. Soc. N. S. W., **76**, pp. 203–224.